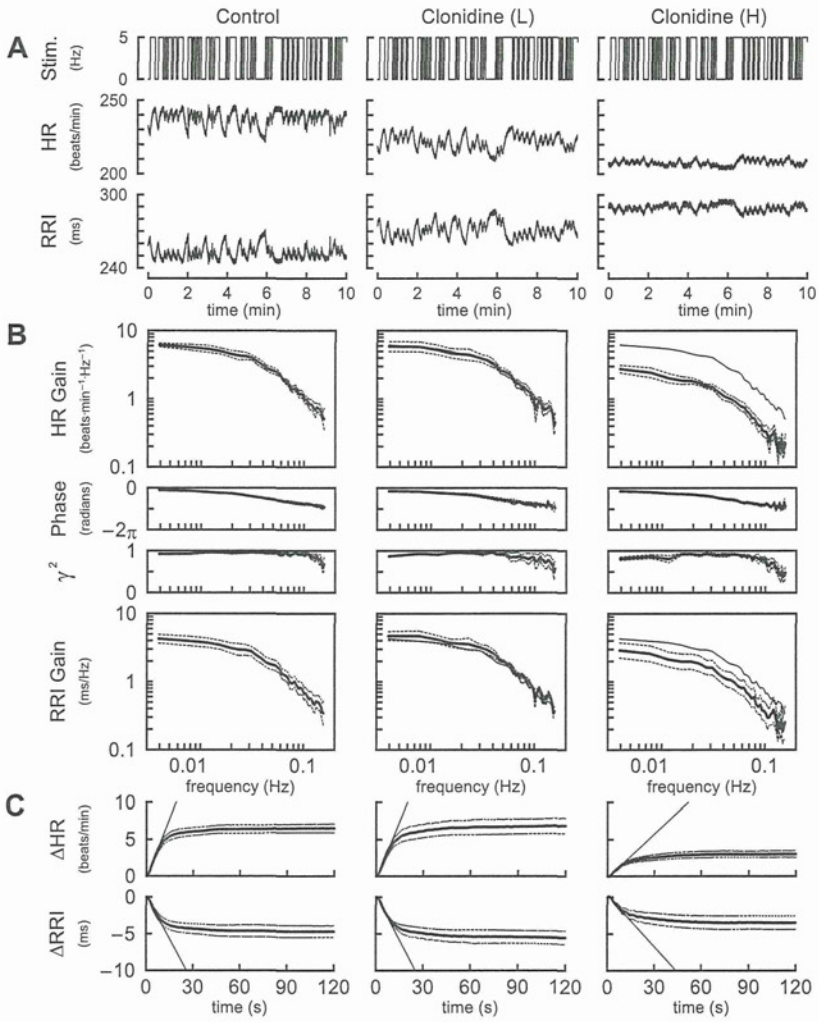

Fig. 3. *A:* representative recordings of cardiac sympathetic nerve stimulation rate (*top*), HR response (*middle*), and RRI response (*bottom*) under conditions of control (*left*), lower-dose clonidine (0.3 $mg \cdot kg^{-1} \cdot h^{-1}$; *middle*), and higher-dose clonidine (1.5 $mg \cdot kg^{-1} \cdot h^{-1}$; *right*) obtained in *protocol 2*. Clonidine activates the presynaptic α_2-adrenergic inhibition independent of the amount of norepinephrine released at the sympathetic nerve terminals. The amplitude of HR variation becomes smaller, and the mean level of HR becomes lower in the presence of higher-dose clonidine. The amplitude of RRI response also became smaller under higher-dose clonidine condition. *B:* transfer functions averaged over all animals in *protocol 2*. HR gain plots (*top*), phase plots (*second*), coherence functions (γ_2, *third*), and RRI gain plots (*bottom*). Lower-dose clonidine does not affect the transfer function significantly. Higher-dose clonidine decreases the dynamic gain in the whole frequency range (0.004 to 0.2 Hz). The fine solid curves in the gain plots (*middle* and *right*) duplicate the mean gain plot (*left*). *C:* step responses of HR (*top*) and RRI (*bottom*) calculated from the corresponding transfer functions. Lower-dose clonidine does not affect the step response significantly. Higher-dose clonidine attenuates the steady-state response accompanied by a decrease in the initial slope of the response (fine oblique line). Bold, solid lines represent the mean, whereas dotted lines indicate means ± SE.

Table 5 summarizes the mean HR and AP obtained from the supplemental protocol. There were no significant differences in mean HR and AP before cardiac sympathetic nerve stimulation. Mean HR was higher in $Bin_{0\text{-}3}$ and $Bin_{0\text{-}5}$ than in $Bin_{0\text{-}1}$ condition. Mean AP did not differ among the three conditions.

Figure 4*B* illustrates the transfer function averaged from the five animals in the supplemental protocol. The contour of HR gain plots showed an approximately downward shift with increase in the stimulus rate of the binary white noise signal, indicating that the augmentation of the HR variation seen in Fig. 4*A* was not proportional to the increase in the stimulus rate. No significant differences were noted in the phase plot. The coherence values were slightly decreased in all frequencies with increase in the stimulus rate of the binary white noise signal, suggesting that the HR response became saturated and the linearity between the stimulation and the HR response was

Table 3. *Mean heart rate and arterial pressure before and during random stimulation of the cardiac sympathetic nerve*

	Control	Clonidine (L)	Clonidine (H)
Heart rate, beats/min			
Before	277±16	250±15	232±20*
During	299±14	271±14	246±27*
Mean arterial pressure, mmHg			
Before	95±6	77±8	113±9
During	96±6	79±9	115±13

Values are means ± SE. Data were obtained after vagal and cardiac sympathetic nerves were cut. *$P < 0.05$ vs. control values by Dunnett's test.

Table 4. *Transfer function parameters and step responses*

	Control	Clonidine (L)	Clonidine (H)
K, $beats \cdot min^{-1} \cdot Hz^{-1}$	6.4±0.8	6.8±1.1	2.7±0.5*
f_N, Hz	0.066±0.017	0.070±0.016	0.059±0.013
ζ	1.56±0.37	1.72±0.23	1.55±0.20
L, s	0.56±0.17	1.24±0.20*	1.03±0.18
Fitting error, %	2.9±1.2	4.2±1.5	5.5±2.3
S, beats/min	6.3±0.8	6.8±1.0	2.8±0.5*
α, $beats \cdot min^{-1} \cdot s^{-1}$	0.56±0.07	0.51±0.04	0.22±0.06*
S/α, s	11.2±0.7	13.1±1.3	13.8±1.2

Values are means ± SE. *$P < 0.05$ vs. control values.

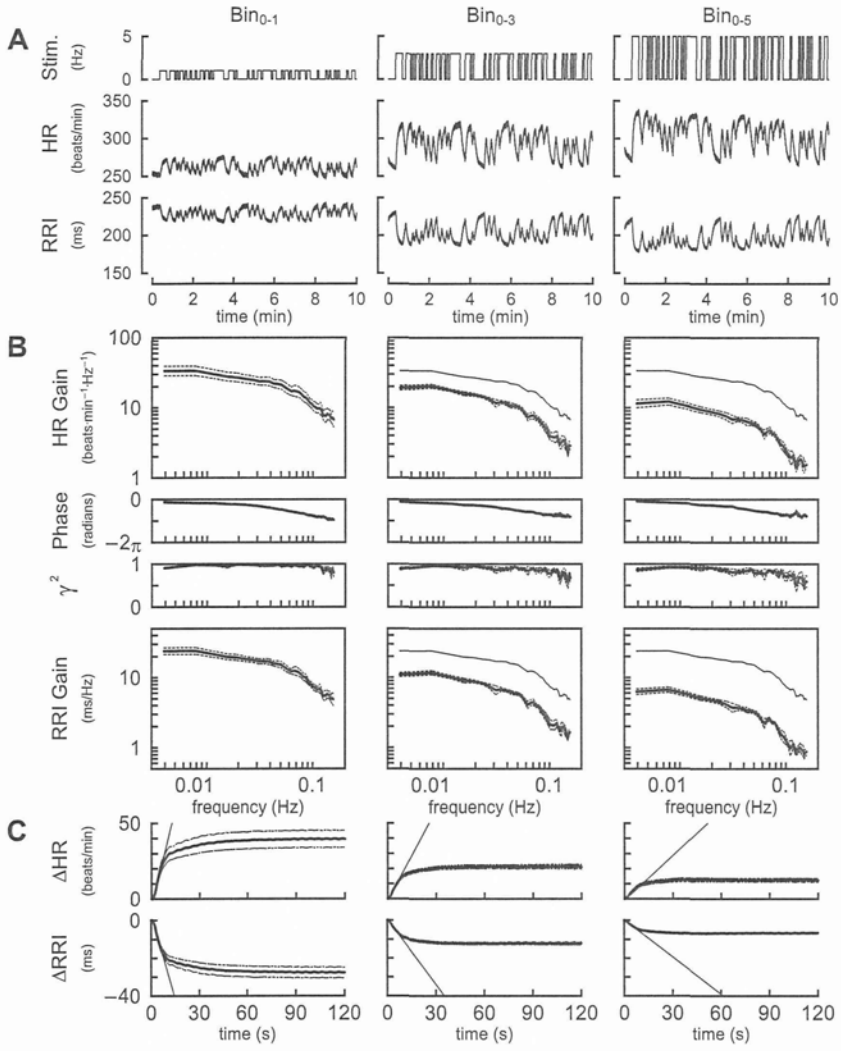

Fig. 4. *A*: representative recordings of cardiac sympathetic nerve stimulation rate (*top*), HR response (*middle*), and RRI response (*bottom*) obtained by differing the stimulus rate of the binary white noise signal. Bin_{0-1}, binary white noise between 0 and 1 Hz; Bin_{0-3}, binary white noise between 0 and 3 Hz; Bin_{0-5}, binary white noise between 0 and 5 Hz. Increasing the stimulus rate of the binary white noise signal augments the magnitude of HR response and increased mean HR. The RRI response was also increased with increasing the stimulus rate. *B:* transfer functions averaged over all animals in the supplemental protocol. HR gain plots (*top*), phase plots (*second*), coherence functions (γ_2, *third*), and RRI gain plots (*bottom*). Increasing the stimulus rate of the binary white noise signal decreases the dynamic gain in the whole frequency range (0.004 to 0.2 Hz). The fine solid curves in the gain plots (*middle* and *right*) duplicate the mean gain plot (*left*). *C:* step responses of HR (*top*) and RRI (*bottom*) calculated from the transfer functions. Increasing the stimulus rate of the binary white noise signal attenuates the steady-state response accompanied by a decrease in the initial slope of the response (fine oblique line). Bold, solid lines represent the mean, whereas dotted lines indicate means ± SE.

slightly reduced in Bin_{0-3} and Bin_{0-5} compared with that in Bin_{0-1} condition. The contour of RRI gain plots also showed approximately downward shift with increasing the stimulus rate of the binary white noise signal.

Figure 4*C* represents the step response of HR to sympathetic nerve stimulation calculated from the transfer functions shown in Fig. 4*B*. The increase in the stimulus rate of the binary white noise signal attenuated the steady-state response and also reduced the initial slope of the response. In the RRI step

Table 5. *Mean heart rate and arterial pressure before and during random stimulation of the cardiac sympathetic nerve*

	Bin_{0-1}	Bin_{0-3}	Bin_{0-5}
Heart rate, beats/min			
Before	268±6	269±7	266±5
During	292±8	330±9*	341±11*
Mean arterial pressure, mmHg			
Before	84±7	82±5	88±12
During	94±7	94±7	95±9

Values are means ± SE. Data were obtained after vagal and cardiac sympathetic nerves were cut. Bin_{0-1}, Bin_{0-3}, and Bin_{0-5}: binary white noise signals of 0–1, 0–3, and 0–5 Hz, respectively. *$P < 0.01$ vs. Bin_{0-1} values by Tukey test. There were no significant differences in parameters between Bin_{0-3} and Bin_{0-5}.

Table 6. *Transfer function parameters and step responses*

	Bin_{0-1}	Bin_{0-3}	Bin_{0-5}
K, beats·min^{-1}·Hz^{-1}	36.2±4.9	20.0±1.1†	11.8±1.1†
f_N, Hz	0.098±0.009	0.079±0.006*	0.078±0.006*
Z	1.56±0.04	1.68±0.04*	1.68±0.05*
L, s	0.95±0.01	0.97±0.01	0.97±0.01
Fitting error, %	4.8±1.1	3.2±0.8	3.5±0.5
S, beats/min	40.9±5.1	22.1±1.6†	12.8±1.4†
α, beats·min^{-1}·s^{-1}	4.23±0.61	2.00±0.21†	1.20±0.17†
S/α, s	9.9±0.5	11.3±0.8	10.8±0.8

Values are means ± SE. †$P < 0.01$ and *$P < 0.05$ vs. Bin_{0-1} values by Tukey test. There were no significant differences in parameters between Bin_{0-3} and Bin_{0-5}.

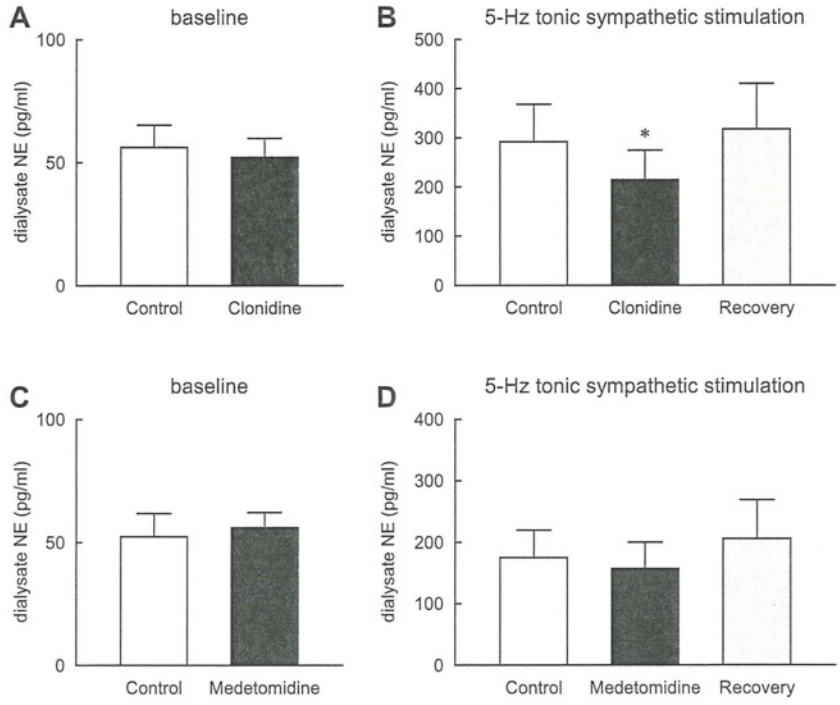

Fig. 5. Effects of clonidine (1.5 mg·kg^{-1}·h^{-1} iv) or medetomidine (1.5 mg·kg^{-1}·h^{-1} iv) on the myocardial interstitial norepinephrine (NE) release in response to 5-Hz tonic cardiac sympathetic nerve stimulation. Data were obtained after sectioning vagal and cardiac sympathetic nerves. Clonidine administration does not affect baseline levels of NE (*A*), but significantly attenuates the stimulation-induced NE release (*B*). *C*: medetomidine administration does not affect baseline levels of NE. *D*: it does not attenuate the stimulation-induced NE release significantly. Values are means ± SE. *$P < 0.05$ from control.

response, the steady-state response was attenuated from -27.6 ± 2.8 to -12.2 ± 0.7 ($P < 0.01$) and -6.7 ± 0.4 ($P < 0.01$) ms during Bin_{0-3} and Bin_{0-5}, respectively. The initial slope was attenuated from -3.0 ± 0.3 to -1.1 ± 0.1 ($P < 0.01$) and -0.65 ± 0.06 ($P < 0.01$) ms/s during Bin_{0-3} and Bin_{0-5}, respectively.

Parameters of the transfer functions and step responses estimated in the supplemental protocol are summarized in Table 6. The steady-state gain of the transfer function and the steady-state response of the corresponding step response decreased with increase in the stimulus rate of the binary white noise sequence. Although the initial slope of the step response significantly decreased with increase in the stimulus rate of the binary white noise signal, the ratio of the steady-state response to the initial slope was unchanged. The natural frequency was lower and the damping coefficient was greater in Bin_{0-3} and Bin_{0-5} than Bin_{0-1} condition. The pure dead time of the transfer function did not differ among the three conditions.

Figure 5 summarizes the results of the supplemental protocol of NE measurement. Baseline levels of myocardial interstitial NE did not differ before and during clonidine administration (Fig. 5*A*). Clonidine administration attenuated the sympathetic stimulation-induced NE release to $75.8 \pm 5.4\%$ of the control ($P < 0.05$) (Fig. 5*B*). Baseline NE levels did not differ before and during medetomidine administration (Fig. 5*C*). Medetomidine did not attenuate the sympathetic stimulation-induced NE release significantly ($92.0 \pm 6.7\%$ of the control, not significant) (Fig. 5*D*).

Simulation Study

To explore possible mechanisms for the observed differences between the presynaptic α_2-adrenergic autoinhibition and the pharmacologic augmentation of the presynaptic inhibition via the α_2-adrenergic receptors, we performed a simulation on the negative feedback regulation of the HR response to the sympathetic nerve stimulation. With reference to Fig. 6*A*, H_{FW} and H_{FB} represent the transfer functions of the forward path and the feedback path, respectively. A step input signal represents the sympathetic nerve stimulation. Both signals from presynaptic α_2-adrenergic autoinhibition and pharmacologic augmentation of the presynaptic inhibition attenuate the input signal via the same α_2-adrenergic receptors. Because the amount of neurotransmitter release cannot become negative, a threshold operator (Th) is added. The threshold operator is described mathematically as follows.

$$\mathrm{Th}(x) = x \text{ when } x > 0, \text{ otherwise } \mathrm{Th}(x) = 0$$

The output from the threshold operator or the amount of neurotransmitter is then fed into H_{FW} to yield the output or change in HR and is also fed into H_{FB} to yield the feedback signal of presynaptic α_2-adrenergic autoinhibition. Since we administered clonidine ~15 min before sympathetic nerve stimulation, the effect of clonidine should have reached the steady state at the time of sympathetic nerve stimulation. Accordingly, we treated the pharmacologic augmentation of the presynaptic inhibition as a constant input. The magnitude of pharmacologic augmentation of the presynaptic inhibition was set arbitrarily to 0.5 to mimic the results of higher dose clonidine in *protocol 2*. The simulation was conducted using Matlab Simulink (The Mathworks, Natick, MA).

Yohimbine administration corresponds to severing the feedback path, i.e., setting $H_{FB} = 0$ in the simulation. Under this condition, the transfer function from the input to output becomes H_{FW}. Therefore, we modeled H_{FW} using the second-order, low-pass filter with pure dead time (*Eq. 3*) with the

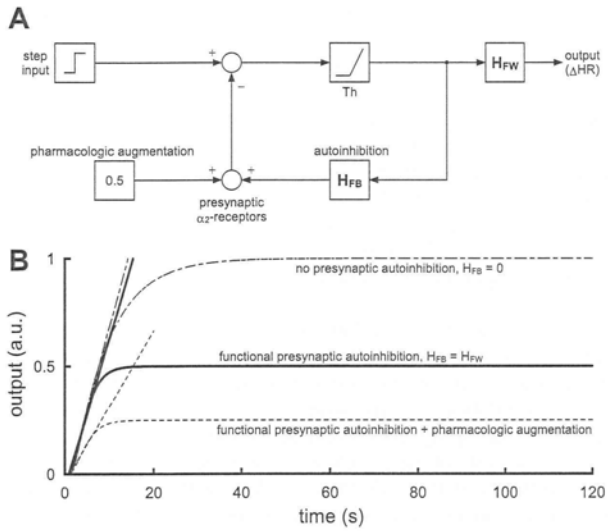

Fig. 6. Possible theoretical explanation for the differential effects of presynaptic α_2-adrenergic autoinhibition and pharmacologic augmentation of presynaptic α_2-adrenergic inhibition on the HR response to sympathetic nerve stimulation. *A:* a simulation model for the HR step response to a step input in the sympathetic nerve activity. H_{FW}, transfer function of the forward path; H_{FB}, transfer function of the feedback path; Th, a threshold operator (see main text for details). *B:* simulation results under conditions of no presynaptic inhibition (dash-dot line; H_{FB} = 0 and pharmacologic augmentation of presynaptic inhibition = 0, corresponding to the yohimbine administration condition), functional presynaptic α_2-adrenergic autoinhibition (solid line; H_{FB} = H_{FW} and pharmacologic augmentation of presynaptic inhibition = 0, corresponding to the control condition), and functional presynaptic α_2-adrenergic autoinhibition plus pharmacologic augmentation of the presynaptic inhibition (dotted line; H_{FB} = H_{FW} and pharmacologic augmentation of presynaptic inhibition = 0.5, corresponding to the higher-dose clonidine condition). The presynaptic α_2-adrenergic autoinhibition does not attenuate the initial slope of the step response. In contrast, the pharmacologic augmentation of the presynaptic inhibition attenuates the initial slope of the step response.

settings of f_N = 0.055, ζ = 1.55, and L = 0.94 (Table 2, yohinbine). The gain was set at unity for simplicity. With this setting, we calculated the output response to the unit step input without the presynaptic inhibition (Fig. 6*B*, dash-dot line, corresponding to the yohimbine condition). The initial slope of the response, calculated from the linear regression analysis described in the method section, was 0.0763 arbitrary units (AU)/s. Next, we set H_{FB} = H_{FW} and performed a simulation of the condition with the presynaptic α_2-adrenergic autoinhibition (Fig. 6*B*, solid line, corresponding to the control condition). The presynaptic α_2-adrenergic autoinhibition attenuates the steady-state response without significantly affecting the initial slope of the response (0.0695 AU/s). Finally, we set the pharmacologic augmentation of the presynaptic inhibition to 0.5 on top of the functioning H_{FB}. The simulation result (Fig. 6*B*, dotted line, corresponding to the higher dose clonidine condition) demonstrates that pharmacologic augmentation of the presynaptic inhibition attenuates the steady-state response accompanied by a reduction in the initial slope of the response (0.0346 AU/s).

DISCUSSION

We compared the blockade and activation of the presynaptic α_2-adrenergic receptors and found a difference between the presynaptic α_2-adrenergic autoinhibition and the pharmacologic augmentation of the presynaptic inhibition in terms of HR response to sympathetic nerve stimulation. The presynaptic α_2-adrenergic autoinhibition showed a limiter-like operation that restricts the steady-state response without affecting the initial slope of the response. In contrast, the pharmacologic augmentation of presynaptic inhibition showed an attenuator-like operation that reduces both the steady-state response and the initial slope of the response.

Comparison of Blocking and Activating the Presynaptic α_2-Adrenergic Receptors

Although the presynaptic α_2-adrenergic negative feedback has been known to attenuate the NE release and HR response to sympathetic nerve stimulation (9, 21, 26, 27, 29, 30, 31), the dynamic nature of the negative feedback remained to be elucidated. As shown in Fig. 2*C*, the blockade of α_2-adrenergic receptors by yohimbine increased the steady-state response without significantly affecting the initial slope of the HR step response (Table 2). That is to say, the presynaptic α_2-adrenergic autoinhibition of the presynaptic inhibition attenuates the steady-state response without sacrificing the rising speed of HR response to sympathetic nerve stimulation under control condition. These characteristics of the presynaptic α_2-adrenergic autoinhibition conform to the limiter-like operation shown in Fig. 1*A*. In contrast, pharmacologic augmentation of the presynaptic inhibition by higher dose clonidine reduced the steady-state response accompanied by a decrease in the initial slope of the HR step response (Fig. 3*C*). The ratio of the steady-state response to the initial slope was not changed significantly by higher dose clonidine (Table 4), suggesting that attenuation of the initial slope was proportional to that of the steady-state response. These characteristics of the pharmacologic augmentation of the presynaptic inhibition conform to the attenuator-like operation shown in Fig. 1*B*. Rapid effector response is one of the most important hallmarks of neural regulation compared with humoral regulation. The findings of the present study suggest that presynaptic α_2-adrenergic autoinhibition, but not pharmacologic augmentation of the presynaptic α_2-adrenergic inhibition, prevents excess NE outflow at the sympathetic nerve terminals without compromising the rapidity of effector response. The simulation results suggest that the initial slope of the response decreases when presynaptic inhibition occurs, independent of the negative feedback mechanism (Fig. 6*B*). On the other hand, the initial slope of the response does not decrease significantly when the presynaptic inhibition occurs through the negative feedback mechanism.

α_2-Adrenergic receptors are classified as α_{2A}-, α_{2B}-, and α_{2C}-subtypes based on gene encodings (26). Furthermore, the different ligand binding characteristics of the α_{2A}-subtype give rise to the pharmacological subtype of α_{2A} in humans, rabbits, and pigs and that of α_{2D} in rats, mice, and guinea pigs (26). The α_{2A} and α_{2D} may be considered as "orthologous" α_2-receptors, with only one being present in any given species (27). In the sympathetic nerve, α_{2A}- and α_{2C}-receptors operate as presynaptic inhibitory autoreceptors, whereas α_{2B}-receptors are located on postsynaptic cells to mediate the effects of catecholamine, such as vasoconstriction (26). In tissue slices from mouse atria, α_{2A}-receptors inhibit NE release from sympathetic nerves primarily at high-stimulation rates (1–2 Hz), whereas

α_{2C}-receptors can operate at very low stimulation rates (0.05–0.1 Hz) (10). Because α_2-receptors in the rabbit heart are characterized as α_{2A}, changes in the transfer function from sympathetic nerve stimulation to HR response observed in the present study are most likely mediated by α_{2A}-receptors.

Clonidine administration (5 μg/kg bolus followed by 30 $\mu g \cdot kg^{-1} \cdot h^{-1}$ iv) attenuated the sympathetic outflow from the central nervous system in rabbits (35). However, lower dose clonidine at 0.3 $mg \cdot kg^{-1} \cdot h^{-1}$ failed to significantly affect the steady-state response or the initial slope of the HR step response in the present study (Fig. 3*B*, Table 4), suggesting a difference in clonidine sensitivity between the central and peripheral sympathetic nervous systems. Another factor that should be taken into account is the operating range of the HR control (i.e., mean HR during dynamic sympathetic stimulation). As an example, tonic vagal stimulation decreased mean HR during dynamic sympathetic stimulation, which increased the dynamic gain of sympathetic HR control via nonlinear sigmoidal input-output nature between autonomic activities and HR (12, 13). Therefore, the decrease in the mean HR during lower dose clonidine, although it was statistically insignificant (Table 3), should have an effect of increasing the dynamic gain of the sympathetic HR control. Such an effect might have counterbalanced the effect of reducing the dynamic gain via presynaptic inhibition during the lower dose clonidine administration. Although higher dose clonidine decreased mean HR before and during sympathetic nerve stimulation, mean AP did not decrease compared with lower dose clonidine (Table 3). The discrepancy between the changes in mean HR and AP may be due to direct vasoconstriction by higher dose clonidine through α-adrenergic stimulation.

Transfer Function Analysis vs. Step Response Analysis

In a previous study, our laboratory performed a transfer function analysis on the sympathetic HR control using a binary white noise signal (12, 23). The transfer function is a frequency-domain representation of the system dynamic characteristics over a wide frequency range and is useful for understanding the behavior of the system in response to a variety of input signals (3, 7, 21). Notwithstanding the theoretical advantages of the transfer function, the frequency-domain representation may be somewhat unfamiliar to most physiologists. Therefore, we calculated the step responses corresponding to the transfer functions. As can be seen in Figs. 2, *B* and *C* and 3, *B* and *C*, changes in transfer function in the lower frequency range reflect the steady-state response in the step response. Changes in transfer function in the higher frequency reflect the initial transient response in the step response. Because the step response and the transfer function are mathematically interchangeable, both the transfer function and the step response provide comparable information on the system dynamic characteristics.

In a previous study, our laboratory has shown that increasing mean stimulus rate of the Gaussian white noise decreased the steady-state gain of the transfer function from sympathetic nerve stimulation to HR without affecting the natural frequency or damping coefficient significantly (23). Increasing the stimulus rate of the binary white noise signal also caused an approximately parallel downward shift in the gain plot (Fig. 4*B*). The transfer function parameters, however, showed a decrease in the natural frequency and an increase in the damping coefficient (Table 6). The higher natural frequency in $Bin_{0\text{-}1}$ than in $Bin_{0\text{-}5}$ condition may account for the higher natural frequency in *protocol 1* ($Bin_{0\text{-}1}$ was used for sympathetic stimulation) than in *protocol 2* ($Bin_{0\text{-}5}$ was used for sympathetic stimulation) observed under control conditions. Notwithstanding the differences in the natural frequency and the damping coefficient, the ratio of the step response to the initial slope was not changed significantly by the difference in the stimulus rate of the binary white noise signal. Therefore, yohimbine-induced changes in the ratio of the step response to the initial slope observed in *protocol 1* (Table 1) cannot be explained by changes in the magnitude of sympathetic effect on HR.

Limitations

The present study has several limitations. First, we performed the experiment under anesthetic conditions. However, because we compared the effects of yohimbine and clonidine on the sympathetic HR control under the same anesthetic

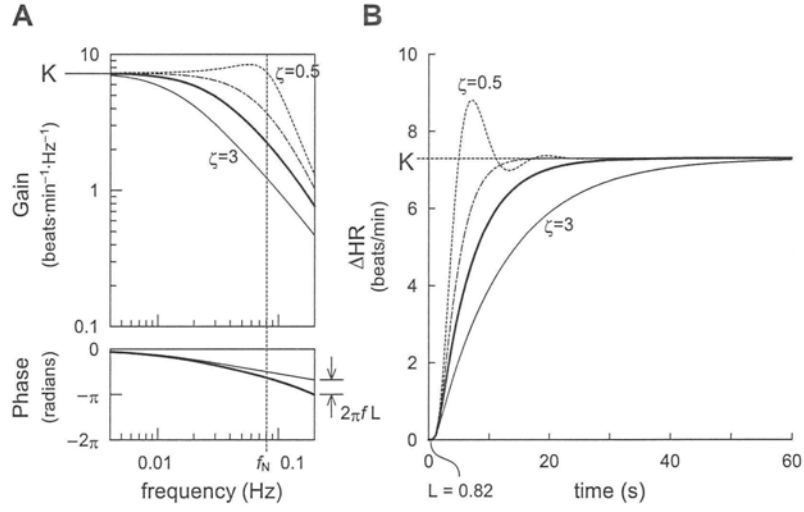

Fig. 7. Schematic explanation for the frequency response of a second-order, low-pass filter with pure dead time (*L*; *A*), and the corresponding step response (*B*). *K*, dynamic gain; f_N, natural frequency; ζ, damping ratio. See APPENDIX for details.

condition, the interpretation of the observed changes in the transfer function may be reasonable. Second, the simulation model in Fig. 6*A* is not the only model that can be applied to the observed results. Although the model is convenient to explain many aspects of the observed results, other models may also be applicable to the present observation. Third, clonidine can affect HR through non-α_2-adrenergic mechanisms. For instance, clonidine caused bradycardia in α_{2ABC}-knockout mouse via direct inhibition of cardiac hyperpolarization-activated cyclic nucleotide-gated pacemaker channels (16). While we tried to use medetomidine instead of clonidine, medetomidine did not attenuate myocardial interstitial NE release in response to sympathetic nerve stimulation significantly, at least, at the same dose as clonidine (Fig. 5). Further studies using other agonists might be required to confirm our observations. Finally, we used a weak stimulus rate (0 to 1 Hz) for the yohimbine protocol. Although we had examined the effect of yohimbine using a strong stimulus rate (0–5 Hz) in a preliminary study, the steady-state gain of the transfer function did not increase much (8.4 ± 1.7 vs. 9.0 ± 1.7 beats·min^{-1}·Hz^{-1}, $n = 3$). Under such strong stimulus condition, the saturation of HR response might have masked the effect of presynaptic inhibition. Therefore, the result of *protocol 1* should be carefully interpreted in view of the existence of a stimulus rate-drug interaction effect.

Conclusions

The presynaptic α_2-adrenergic autoinhibition attenuates the dynamic HR response to sympathetic nerve stimulation in the low-frequency range (0.004–0.04 Hz) but not in the high-frequency range (0.05–0.15 Hz). In the time domain, the presynaptic α_2-adrenergic autoinhibition attenuates the steady-state response without affecting the slope of the response in the HR step response (a limiter-like operation). In contrast, pharmacologic augmentation of presynaptic α_2-adrenergic inhibition attenuates the dynamic HR response to sympathetic nerve stimulation in a frequency-independent manner. In the time domain, pharmacologic augmentation of the presynaptic inhibition attenuates not only the steady-state response but also the initial slope of the HR step response (an attenuator-like operation). Presynaptic α_2-adrenergic autoinhibition would be favorable for limiting excess NE outflow at the sympathetic nerve terminals without compromising the rapidity of effector response.

APPENDIX

Mathematical Modeling of the Sympathetic HR Response

To describe the estimated transfer function, we used a second-order, low-pass filter with pure dead time (L). Figure 7*A* shows the frequency response of a second-order, low-pass filter with L. Figure 7*B* shows the corresponding step response. The step response is calculated for 1-Hz sympathetic nerve stimulation. The steady-state gain (K) of the transfer function represents the value of transfer gain as the frequency approaches zero. The K corresponds to the steady-state response in the step-response representation. The natural frequency (f_N) determines the upper frequency limit of the low-pass filter. For instance, if the f_N were 10 times higher, the frequency axis in Fig. 7*A* would have to be scaled by a factor of 10, indicating that the system could respond to 10-fold higher frequency input. The phase plot in Fig. 7*A* indicates that, at the f_N, the output is delayed by $\pi/2$ radians relative to the input, in the absence of the L. The maximum phase delay of the second-order, low-pass filter is π radians in the absence of L. The L is needed to account for the phase difference between the estimated transfer function and the second-order, low-pass filter. In Fig. 7*B*, the L corresponds to the time difference between the onset of the step input and the onset of the response. The damping coefficient (ζ) characterizes the system response around the f_N. As an example, the gain plot shows a slight peak around f_N when $\zeta = 0.5$ (dotted line). Figure 7*B* shows that a ζ of 0.5 causes an initial overshoot in response to a step change in the input. A system with $\zeta < 1$ is called underdamped. On the other hand, the gain plot shows more gradual decrease around f_N when $\zeta = 3$ (fine solid line). Figure 7*B* shows that the system responds sluggishly when $\zeta = 3$. A system with $\zeta > 1$ is called overdamped. A system with $\zeta = 1$ is called critically damped (dash-dot line). The ζ of the estimated transfer functions ranged from 1.55 to 1.72 in the present study, indicating that the sympathetic HR control system is overdamped. The solid line represents the second-order, low-pass filter with $\zeta = 1.64$ and $L = 0.82$ that is derived from the mean value obtained under control condition in *protocol 1*.

GRANTS

This study was supported by "Health and Labour Sciences Research Grant for Research on Advanced Medical Technology," "Health and Labour Sciences Research Grant for Research on Medical Devices for Analyzing, Supporting and Substituting the Function of Human Body," and "Health and Labour Sciences Research Grant H18-Iryo-Ippan-023" from the Ministry of Health, Labour and Welfare of Japan; "Program for Promotion of Fundamental Studies in Health Science" from the National Institute of Biomedical Innovation; and "Ground-based Research Announcement for Space Utilization" promoted by the Japan Space Forum.

REFERENCES

1. **Altman JD, Trendelenburg AU, MacMillan L, Bernstein D, Limbird L, Starke K, Kobilka BK, Hein L.** Abnormal regulation of the sympathetic nervous system in α_{2A}-adrenergic receptor knockout mice. *Mol Pharmacol* 56: 154–161, 1999.
2. **Bendat JS, Piersol AG.** Single-input/output relationships. In: *Random Data Analysis and Measurement Procedures* (3rd Ed.). New York: Wiley, 2000, p. 189–217.
3. **Berger RD, Saul JP, Cohen RJ.** Transfer function analysis of autonomic regulation. I. Canine atrial rate response. *Am J Physiol Heart Circ Physiol* 256: H142–H152, 1989.
5. **Brigham EO.** FFT transform applications. In: *The Fast Fourier Transform and Its Applications*. Englewood Cliffs, NJ: Prentice-Hall, 1988, p. 167–203.
6. **Buhler FR, Bolli P, Amann WF, Erne P, Kiowski W.** Sympathetic nervous system in essential hypertension and antihypertensive response to α_2-adrenoceptor stimulation. *J Cardiovasc Pharmacol* 6: S753–S756, 1984.
7. **Franklin GF, Powell JD, and Emani-Naeini A.** Dynamic models and dynamic response. In: *Feedback Control of Dynamic Systems* (2nd Ed.). Boston, MA: Addison-Wesley, 1991, p. 17–144.
8. **Glantz SA.** *Primer of Biostatistics* (5th Ed.). New York: McGraw-Hill, 2002.
9. **Grossman E, Chang PC, Hoffman A, Tamrat M, Goldstein DS.** Evidence for functional α_2-adrenoceptors on vascular sympathetic nerve endings in the human forearm. *Circ Res* 69: 887–897, 1991.
10. **Hein L, Altman JD, Kobilka BK.** Two functionally distinct α2-adrenergic receptors regulate sympathetic neurotransmission. *Nature* 402: 181–184, 1999.
11. **Jie K, van Brummelen P, Vermey P, Timmermans PB, van Zwieten PA.** Modulation of noradrenaline release by peripheral presynaptic α_2-adrenoceptors in humans. *J Cardiovasc Pharmacol* 9: 407–413, 1987.
12. **Kawada T, Ikeda Y, Sugimachi M, Shishido T, Kawaguchi O, Yamazaki T, Alexander J Jr, Sunagawa K.** Bidirectional augmentation of heart rate regulation by autonomic nervous system in rabbits. *Am J Physiol Heart Circ Physiol* 271: H288–H295, 1996.
13. **Kawada T, Sugimachi M, Shishido T, Miyano H, Sato T, Yoshimura R, Miyashita H, Nakahara T, Alexander J Jr, Sunagawa K.** Simultaneous identification of static and dynamic vagosympathetic interactions in regulating heart rate. *Am J Physiol Regul Integr Comp Physiol* 276: R782–R789, 1999.

14. **Kawada T, Yamazaki T, Akiyama T, Sato T, Shishido T, Sugimachi M, Inagaki M, Alexander J Jr, Sunagawa K.** Liquid chromatographic determination of myocardial interstitial epinephrine. *J Chromatogr B Biomed Sci Appl* 714: 375–378, 1998.
15. **Kawada T, Yamazaki T, Akiyama T, Sato T, Shishido T, Yoshimura R, Inagaki M, Tatewaki T, Sugimachi M, Sunagawa K.** Local epinephrine release in the rabbit myocardial interstitium in vivo. *J Auton Nerv Syst* 78: 94–98, 2000.
16. **Knaus A, Zong X, Beetz N, Jahns R, Lohse MJ, Biel M, Hein L.** Direct inhibition of cardiac hyperpolarization-activated cyclic nucleotide-gated pacemaker channels by clonidine. *Circulation* 115: 872–880, 2007.
17. **Langer SZ.** 25 years since the discovery of presynaptic receptors, present knowledge and future perspectives. *Trends Pharmacol Sci* 18: 95–99, 1997.
18. **Langer SZ.** Presence and physiological role of presynaptic inhibitory α_2-adrenoreceptors in guinea pig atria. *Nature* 294: 671–672, 1981.
19. **Langer SZ, Adler-Graschinsky E, Giorgi O.** Physiological significance of α-adrenoceptor-mediated negative feedback mechanism regulating noradrenaline release during nerve stimulation. *Nature* 265: 648–650, 1977.
20. **Langer SZ.** Presynaptic regulation of catecholamine release. *Biochem Pharmacol* 23: 1793–1800, 1974.
21. **Marmarelis PZ, Marmarelis VZ.** The white noise method in system identification. In: *Analysis of Physiological Systems*. New York: Plenum, 1978, p. 131–221.
22. **Miyamoto T, Kawada T, Yanagiya Y, Takaki H, Inagaki M, Sugimachi M, Sunagawa K.** Cardiac sympathetic nerve stimulation does not attenuate dynamic vagal control of heart rate via α-adrenergic mechanism. *Am J Physiol Heart Circ Physiol* 287: H860–H865, 2004.
23. **Nakahara T, Kawada T, Sugimachi M, Miyano H, Sato T, Shishido T, Yoshimura R, Miyashita H, Inagaki M, Alexander J Jr, Sunagawa K.** Neuronal uptake affects dynamic characteristics of heart rate response to sympathetic stimulation. *Am J Physiol Regul Integr Comp Physiol* 277: R140–R146, 1999.
24. **Niederhoffer N, Hein L, Starke K.** Modulation of the baroreceptor reflex by α_{2A}-adrenoceptors, a study in α_{2A} knockout mice. *Br J Pharmacol* 141: 851–859, 2004.
25. **Pelayo F, Dubocovich ML, Langer SZ.** Regulation of noradrenaline release in the rat pineal through a negative feedback mechanism mediated by presynaptic α-adrenoceptors. *Eur J Pharmacol* 45: 317–318, 1977.
26. **Philipp M, Brede M, Hein L.** Physiological significance of α_2-adrenergic receptor subtype diversity, one receptor is not enough. *Am J Physiol Regul Integr Comp Physiol* 283: R287–R295, 2002.
27. **Rump LC, Bohmann C, Schaible U, Schöllhorn J, Limberger N.** α2C-Adrenoceptor-modulated release of noradrenaline in human right atrium. *Br J Pharmacol* 116: 2617–2624, 1995.
27a. **Schwartz DD.** Activation of alpha-2 adrenergic receptors inhibits norepinephrine release by a pertussis toxin-insensitive pathway independent of changes in cytosolic calcium in cultured rat sympathetic neurons. *J Pharmacol Exp Ther* 282: 248–255, 1997.
28. **Sinclair MD.** A review of the physiological effects of α2-agonists related to the clinical use of medetomidine in small animal practice. *Can Vet J* 44: 885–897, 2003.
29. **Starke KM, Gothert M, Kilbinger H.** Modulation of neurotransmitter release by presynaptic autoreceptors. *Physiol Rev* 69: 864–989, 1989.
30. **Starke KM.** Presynaptic α-autoreceptors. *Rev Physiol Biochem Pharmacol* 107: 73–146, 1987.
31. **Starke K, Langer SZ.** A note on terminology for presynaptic receptors. In: *Presynaptic Receptors*, edited by Langer SZ, Starke K, and Dubocovich ML. Oxford, UK: Pergamon 1979, p. 1–3.
32. **Starke K, Endo T, Taube HD.** Pre- and post-synaptic components in effect of drugs with α-adrenoceptor affinity. *Nature* 254: 440–441, 1975.
33. **Starke K.** Alpha sympathomimetic inhibition of adrenergic and cholinergic transmission in the rabbit heart. *Naunyn Schmiedebergs Arch Pharmacol* 274: 18–45, 1972.
34. **Szabo B, Schramm A, Starke K.** Effect of yohimbine on renal sympathetic nerve activity and renal norepinephrine spillover in anesthetized rabbits. *J Pharmacol Exp Ther* 260: 780–788, 1992.
35. **Szabo B, Hedler L, Starke K.** Peripheral presynaptic and central effects of clonidine, yohimbine and rauwolscine on the sympathetic nervous system in rabbits. *Naunyn-Schmiedeberg's Arch Pharmacol* 340: 648–657, 1989.
37. **Vizi ES, Somogyi GT, Hadhazy P, Knoll J.** Effect of duration and frequency of stimulation on the presynaptic inhibition by α-adrenoceptor stimulation of the adrenergic transmission. *Naunyn-Schmiedeberg's Arch Pharmacol* 280: 79–91, 1973.
38. **Westfall TC.** Local regulation of adrenergic neurotransmission. *Physiol Rev* 57: 659–728, 1977.

Behavioral/Systems/Cognitive

Reverse of Age-Dependent Memory Impairment and Mitochondrial DNA Damage in Microglia by an Overexpression of Human Mitochondrial Transcription Factor A in Mice

Yoshinori Hayashi,[1]* Masayoshi Yoshida,[2,4]* Mayumi Yamato,[3]* Tomomi Ide,[2] Zhou Wu,[1] Mayumi Ochi-Shindou,[1] Tomotake Kanki,[4] Dongchon Kang,[4] Kenji Sunagawa,[2] Hiroyuki Tsutsui,[5] and Hiroshi Nakanishi[1]

[1]Laboratory of Oral Aging Science, Faculty of Dental Sciences, [2]Department of Cardiovascular Medicine, Graduate School of Medical Sciences, [3]Department of REDOX Medicinal Science, Graduate School of Pharmaceutical Sciences, [4]Department of Clinical Chemistry and Laboratory Medicine, Kyushu University, Fukuoka 812-8582, Japan, and [5]Department of Cardiovascular Medicine, Hokkaido University Graduate School of Medicine, Sapporo 060-8638, Japan

Mitochondrial DNA (mtDNA) is highly susceptible to injury induced by reactive oxygen species (ROS). During aging, mutations of mtDNA accumulate to induce dysfunction of the respiratory chain, resulting in the enhanced ROS production. Therefore, age-dependent memory impairment may result from oxidative stress derived from the respiratory chain. Mitochondrial transcription factor A (TFAM) is now known to have roles not only in the replication of mtDNA but also its maintenance. We herein report that an overexpression of TFAM in HeLa cells significantly inhibited rotenone-induced mitochondrial ROS generation and the subsequent NF-κB (nuclear factor-κB) nuclear translocation. Furthermore, TFAM transgenic (TG) mice exhibited a prominent amelioration of an age-dependent accumulation of lipid peroxidation products and a decline in the activities of complexes I and IV in the brain. In the aged TG mice, deficits of the motor learning memory, the working memory, and the hippocampal long-term potentiation (LTP) were also significantly improved. The expression level of interleukin-1β (IL-1β) and mtDNA damages, which were predominantly found in microglia, significantly decreased in the aged TG mice. The IL-1β amount markedly increased in the brain of the TG mice after treatment with lipopolysaccharide (LPS), whereas its mean amount was significantly lower than that of the LPS-treated aged wild-type mice. At the same time, an increased mtDNA damage in microglia and an impaired hippocampal LTP were also observed in the LPS-treated aged TG mice. Together, an overexpression of TFAM is therefore considered to ameliorate age-dependent impairment of the brain functions through the prevention of oxidative stress and mitochondrial dysfunctions in microglia.

Key words: mitochondria DNA; transcription factor A; oxidative stress; aging; memory impairment; microglia

Introduction

It is widely believed that oxidative stress and inflammation are major causative factors for a progressive decline in motor and memory functions during aging in humans and animals (Forster et al., 1996; Navarro et al., 2002). Behavioral dysfunctions associated with aging are also postulated to be associated with a decreased activity of mitochondrial electron transfer complexes with aging (Navarro et al., 2004, 2005). Furthermore, increased intracellular reactive oxygen species (ROS) activate microglia, which are representative resident mononuclear phagocyte populations in the brain, to induce an increased production of inflammatory mediators (Pawate et al., 2004; Qin et al., 2005). ROS generated in close proximity and in large concentrations by the mitochondrial respiratory chain cause oxidation of unsaturated fatty acid, proteins, and DNA. Mitochondrial DNA (mtDNA) is highly susceptible to damage produced by ROS because of its close proximity to ROS generation through the respiratory chain and its paucity of protective histones. Furthermore, there is little capacity for DNA repair in the mitochondria. During aging, a large number of mtDNA mutations accumulate in various tissues including the brain, thus leading to dysfunction of the respiratory

Received March 3, 2008; revised July 7, 2008; accepted July 15, 2008.

This work was supported by Grants-in-Aid for Scientific Research and Grant-in-Aid for Scientific Research on Priority Area from the Ministry for Education, Science, and Culture, Japan; a Labor Science Research Grant for Comprehensive Research in Aging and Health Labor and Welfare of Japan; and the Uehara Research Foundation. We thank Prof. V. Hugh Perry (CNS Inflammation Group, School of Biological Sciences, University of Southampton, Southampton, UK) for his critical reading of this manuscript. We also thank Keiko Kurakazu for technical assistance and Drs. Atsushi Fukuoh and Kippei Ohgaki for technical advice.

*Y.H., M. Yoshida, and M. Yamato contributed equally to this work.

Correspondence should be addressed to either of the following: Dr. Tomomi Ide, Department of Cardiovascular Medicine, Kyushu University Graduate School of Medicine, 3-1-1, Maidashi, Higashi-ku, Fukuoka 812-8582, Japan, E-mail: tomomi_i@cardiol.med.kyushu-u.ac.jp; or Dr. Hiroshi Nakanishi, Laboratory of Oral Aging Science, Faculty of Dental Sciences, Kyushu University, 3-1-1, Maidashi, Higashi-ku, Fukuoka 812-8582, Japan, E-mail: nakan@dent.kyushu-u.ac.jp.

M. Ochi-Shindou's present address: Neurobiology Research Unit, Okinawa Institute of Science and Technology, Okinawa 904-2234, Japan.

DOI:10.1523/JNEUROSCI.1957-08.2008

 0270-6474/08/288624-11$15.00/0

chain. Finally, deficits in the respiratory chain result in the enhanced ROS production, culminating in age-dependent memory impairments (Corral-Debrinski et al., 1992; Lin et al., 2002). Therefore, the vulnerability of mtDNA to ROS is a major determinant factor for deficits in the brain functions in aging.

Mitochondrial transcription factor A (TFAM) is a nucleus-encoded protein that binds upstream of the light-strand and heat-strand promoters of mtDNA and promotes the transcription of mtDNA (Parisi and Clayton, 1991). Moreover, there is increasing evidence that TFAM plays an important role in maintaining mtDNA and regulating its copy number. The amount of mtDNA is closely correlated with the amount of TFAM but not with the transcription level, and the majority of TFAM molecules are involved in architecturally maintaining the higher structure of mtDNA (Kanki et al., 2004b). More recently, transgenic mice that overexpressed human TFAM under control of the β-actin promoter were generated and showed an increased copy number of mtDNA in the myocardium and the protection of the heart from mitochondrial dysfunction (Ikeuchi et al., 2005). The improvement in mitochondrial respiratory function may thus lead to an amelioration of the chronic process of remodeling by decreasing the mitochondrial ROS generation. The brain has a higher demand for oxygen; therefore, it is possible that increased oxidative stress and consequent mtDNA mutations may lead to the accumulation of lipid peroxidation products. Furthermore, it is reasonable to speculate that such TFAM overexpression may also inhibit the mitochondrial ROS generation through a reduction of the mtDNA mutations, which may retard the motor and memory functions.

To address this issue, the effects of TFAM overexpression on age-dependent deficits in brain functions were examined using human TFAM transgenic (TG) mice. The present study showed a significant improvement in the age-dependent memory impairments in TG mice because of a marked reduction in both oxidative stress and inflammation in the brain.

Materials and Methods

All experimental procedures of this study were approved by the Animal Care and Use Committee of Kyushu University.

Overexpression of TFAM in HeLa cells using the tetracycline-regulation system. Tetracycline-regulated TFAM-overexpressing cell lines were produced as previously reported (Parisi and Clayton, 1991). The cells were grown in DMEM containing 10% fetal bovine serum, 400 mg/ml Geneticin (G418), and 200 mg/ml hygromycin B, with or without 1 mg/ml doxycycline (DC) and maintained at 37°C in humidified air with 5% CO_2. The cells were then seeded in 24-well dishes and the culture medium was replaced after 24 h with serum-free DMEM containing 400 mg/ml G418 and 200 mg/ml hygromycin B, with or without 1 mg/ml DC. After 24 h, the cells were treated for 6 h with 0.001% of 1 mol/L rotenone dissolved in ethanol. The protein levels of human TFAM in the soluble fractions of HeLa cells in the presence and absence of DC were analyzed by immunoblotting.

Rotenone-induced ROS measurement. Intracellular ROS was measured by a ROS-sensitive fluorescent probe, 2,7-diamino-10-ethyl-9-phenyl-9,10-dihydrophenanthridine (DHE), in tetracycline-regulated HeLa cells. The cells were plated in 96-well culture dishes and cultured for 24 h at 37°C in humidified air with 5% CO_2, followed by incubation in serum-free medium for another 24 h. Next, the cells were treated with 1 μmol/L rotenone for 5.5 h and then with 2 μmol/L DHE for 30 min. The fluorescent intensity was determined immediately at excitation wavelength of 485 nm and emission wavelength of 530 nm on a fluorescent plate reader. The cellular images for DHE oxidation were observed using confocal laser-scanning microscope (CLSM) (LSM510MET; Carl Zeiss).

CLSM images for nuclear factor-κB nuclear translocation. Tetracycline-regulated TFAM-overexpressing HeLa cells were seeded in 24-well dish at a density of 10^3 cells/mm^2. The culture medium was replaced after 24 h with serum-free DMEM medium containing 400 mg/ml G418 and 200 mg/ml hygromycin B, with or without 1 mg/ml DC. After 24 h, the cells were treated for 6 h with 0.001% (final concentration in medium) of 1 mol/L rotenone dissolved in ethanol. After treatment with rotenone or vehicle, the cells were fixed with 4% paraformaldehyde and then incubated with mouse anti-p65 monoclonal antibody (Santa Cruz Biotechnology; AH Diagnostics) in bovine serum albumin (BSA)/PBS overnight at 4°C, washed three times with PBS, and then incubated with a secondary Alexa 488 goat anti-mouse IgG antibody in BSA/PBS for 1 h at room temperature. After three washes, the nuclei of cells were counterstained with propidium iodide (Sigma-Aldrich). The cells showing bright staining for p65 in the nucleus were scored, and the results were presented as a percentage of the number of cells with nuclear factor-κB (NF-κB) nuclear translocation to the total number of cells examined.

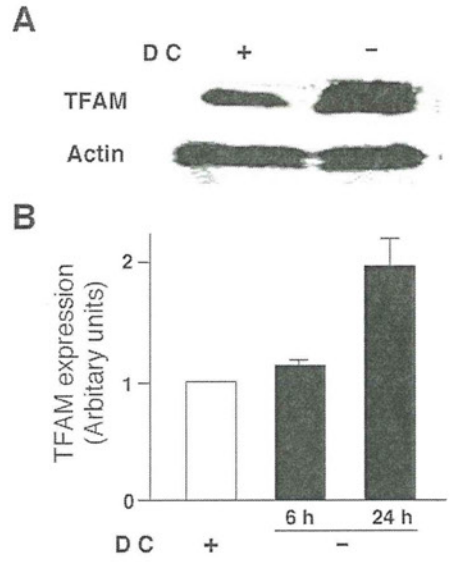

Figure 1. Protein levels of human TFAM overexpressed by the tetracycline-off system in HeLa cells. ***A***, Immunoblot analysis of human TFAM expressed in HeLa cells cultured with and without DC for 24 h. ***B***, The mean protein level of human TFAM in HeLa cells cultured with and without DC for 6 and 24 h. The mean relative immunoreactivity of each protein band was determined using the level of actin as an internal control. Each column and bar represent the mean and SEM of three experiments, respectively.

Animals. The methods for generating TG mice that overexpressed human TFAM has been described previously (Ikeuchi et al., 2005). The animals were housed under 12 h light/dark cycle (lights on at 8:00 A.M.) with access to food and water *ad libitum*. All mice were handled daily for 5 d before the start of the experiment to minimize stress reactions to manipulation.

Immunoblotting. Antibodies against human TFAM and mouse Tfam were produced by immunizing rabbits with recombinant glutathione *S*-transferase-tagged human TFAM and mouse Tfam. The protein levels of human TFAM and mouse endogenous TFAM were analyzed in the soluble fractions of brain tissue homogenates as previously described (Lin et al., 2002).

Thiobarbituric acid reactive substances. Twenty male C57BL/6 mice [wild type (WT) and TG] of the following age groups: young (2 months of age; WT, $n = 5$; TG, $n = 5$) and aged (24 months of age; WT, $n = 5$; TG, $n = 5$) were used for the measurement of thiobarbituric acid reactive substances (TBARS). The homogenates of whole brains were mixed with 0.4% SDS, 7.5% acetic acid adjusted to pH 3.5 with NaOH, and 0.3% thiobarbituric acid. The mixture was kept at 5°C for 60 min and then heated at 100°C for 60 min. After cooling, the mixture was extracted with distilled water and *n*-butanol:pyridine (15:1, v/v) and centrifuged at 16,000× *g* for 10 min. The fluorescence of the supernatant was measured at excitation and emission wavelengths of 510 and 550 nm, respectively, using GENios Pro (Tecan). The standard was prepared using TEP (1,1,3,3-tetraethoxypropane).

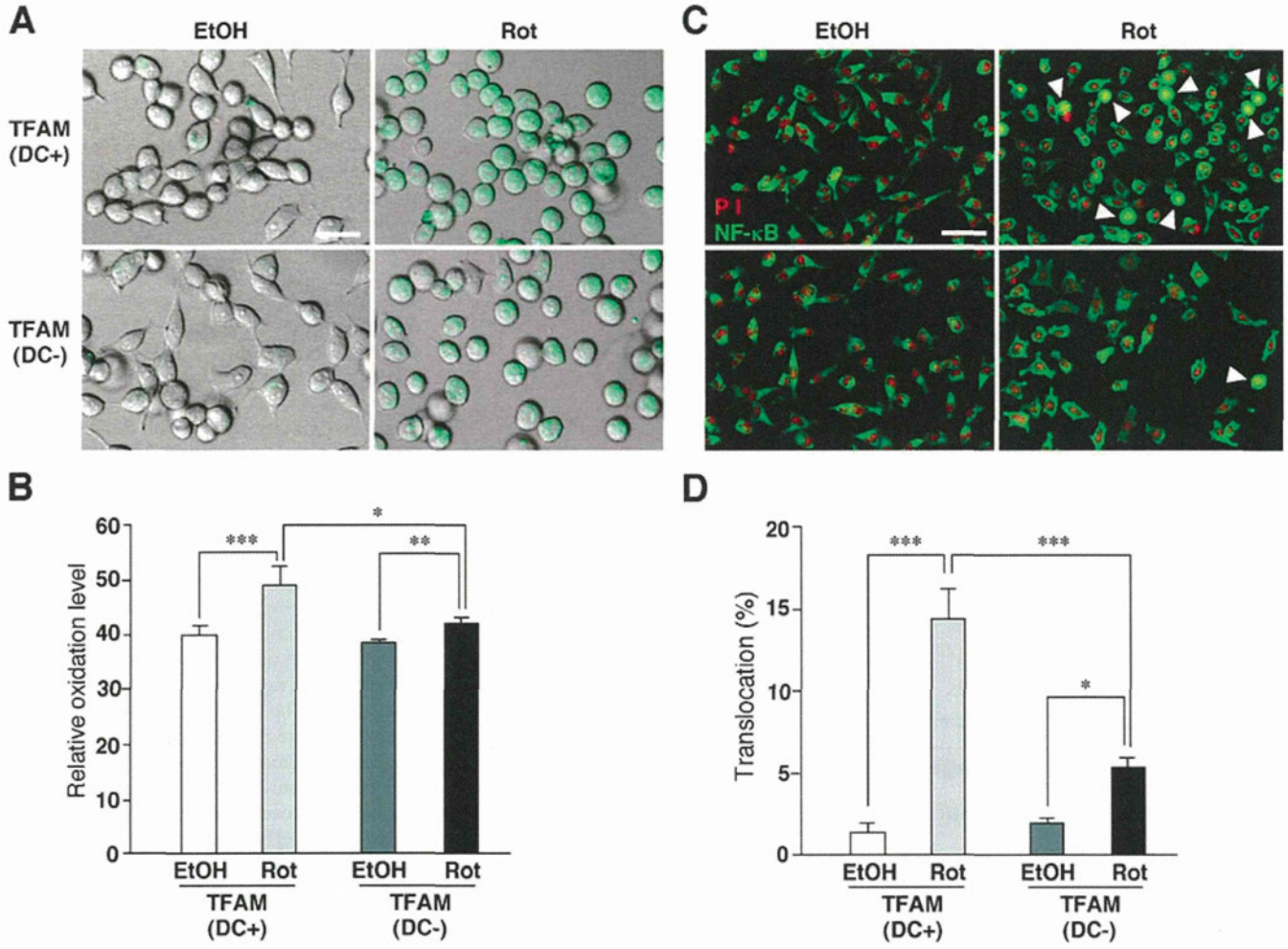

Figure 2. Effects of an overexpression of TFAM by the tetracycline-off system on rotenone-induced intracellular ROS generation and NF-κB nuclear translocation in HeLa cells. ***A***, CLMS images of rotenone-induced intracellular ROS generation measured using a ROS-sensitive dye (green), DHE, in HeLa cells cultured with or without DC. Scale bar, 20 μm. ***B***, The mean DHE oxidation levels in HeLa cells cultured with or without DC after treatment with EtOH or rotenone. Each column and bar represent the mean ± SEM of six experiments. The asterisks indicate a significant difference between two groups (*$p < 0.05$; **$p < 0.01$; ***$p < 0.001$). ***C***, NF-κB (green) and propidium iodide (PI)-stained nuclei (red) in HeLa cells cultured with or without DC after the treatment with EtOH or rotenone. The arrowheads show HeLa cells with the nuclear translocated NF-κB. Scale bar, 50 μm. ***D***, The mean percentage of the NF-κB nuclear translocation in HeLa cells cultured with or without DC after the treatment with EtOH or rotenone. Each column and bar represent the mean ± SEM of nine experiments. The asterisks indicate significant differences between two groups (*$p < 0.05$; ***$p < 0.001$). Rot, Rotenone.

Mitochondrial enzyme activities. Twenty male C57BL/6 mice (WT and TG) of the following age groups: young (2 months of age; WT, $n = 5$; TG, $n = 5$) and aged (24 months of age; WT, $n = 5$; TG, $n = 5$) were used to measure the mitochondrial enzyme activities. The specific activity of mitochondrial complex enzymes, including complexes I, II, III, and IV, was measured in mitochondria isolated from whole brains of each group as described previously (Ide et al., 1999). The specific activity of rotenone-sensitive NADH-ubiquinone oxidoreductase (complex I) was measured by reduction of the ubiquinone analog decylubiquinone. For the activity of succinate ubiquinone oxidoreductase (complex II), the reduction of 2,6-dichlorophenolindophenol when coupled to complex II-catalyzed reduction of decylubiquinone was measured. For the specific activity of ubiquinol/cytochrome *c* oxidoreductase (complex III), the reduction of cytochrome *c* catalyzed by complex III in the presence of reduced decylubiquinone was monitored. The specific activity of cytochrome *c* oxidase (complex IV) was measured by following the oxidation of reduced cytochrome *c*, which was prepared in the presence of dithionite. All enzymatic activities were expressed as nanomoles per minute per milligram of protein.

Immunohistochemistry. Twenty-four male C57BL/6 mice (WT and TG) of the following age groups: young (2–4 months of age; WT, $n = 6$; TG, $n = 6$) and aged (20–24 months of age; WT, $n = 6$; TG, $n = 6$) were used for the immunohistochemical analyses. WT and TG mice of both young and aged groups were anesthetized with sodium pentobarbital (40 mg/kg, i.p.) and killed by intracardiac perfusion with isotonic saline followed by PBS, pH 7.4. After perfusion, the brain was removed and further fixed by immersion in 4% paraformaldehyde overnight at 4°C, and then immersed in 30% sucrose for 24 h at 4°C. Floating coronal sections (10 μm thick) of the hippocampus were prepared by a cryostat and stained with anti-human TFAM, anti-8-oxo-deoxyguanosine (8-oxo-dG) (NOF Corporation), anti-4-hydroxy-2-nonenal (HNE) (Alpha Diagnostic), and anti-interleukin-1β (IL-1β) (Santa Cruz Biotechnology) for 3 d at 4°C. To detect any oxidative damage in the mitochondrial DNA rather than in the nuclear DNA, the sections were directly treated with anti-8-oxo-dG antibody without treatment of HCl as described previously (Kajitani et al., 2006). After washing with PBS, the sections were stained using the avidin–biotin–peroxidase complex method (Vector Laboratories). After washing with PBS, the sections were reacted with 0.015% 3′,3-diaminobenzidine/0.4% $(NH_4)_2Ni(SO_4)_2$/0.09% H_2O_2/0.1 mol/L Tris-buffered saline for 5–10 min. The sections were rinsed thoroughly with PBS, mounted, and coverslipped. As negative controls, the sections were incubated with nonimmune rabbit IgG or mouse IgG instead of the first antibody and processed in the same manner as described above.

For double fluorescent staining, the floating sections were stained with the following combinations of the first antibodies for 48 h at 4°C: anti-